Uniform Suction for the Reduction of the Trailing Edge Noise

Máté Szőke*,
University of Bristol, Bristol, BS8 1TR, UK
Virginia Tech, Blacksburg, VA, 24061, USA

Daniele Fiscaletti† and Mahdi Azarpeyvand‡
University of Bristol, Bristol, BS8 1TR, UK

Uniform inclined suction from a spanwise slot is applied upstream of a trailing edge on a zero pressure gradient flat plate with the aim of reducing trailing edge noise. The effects of the flow treatment on the turbulence statistics are experimentally investigated downstream of the flow control section using hot-wire anemometry. Surface pressure measurements from flush-mounted microphones are used to estimate the far-field trailing edge noise. The area of the flow control is kept constant, while the flow suction velocity and the angle of suction are varied. We examine four angles of flow suction velocity, namely $\alpha = 30^\circ, 50^\circ, 70^\circ$ and 90° alongside a wide range of flow control severities. It is found that flow suction changes the overall structure of the flow. Both the boundary layer thickness and the momentum thickness increases as a result of flow suction. The mean velocity profiles non-dimensionalized by the inner units show that flow suction increases the extent of the viscous region, while the logarithmic region progressively reduces its size with increasing the flow suction severity. At sufficiently high suction rates, the logarithmic region disappears, which is an evidence of flow laminarisation. Flow suction efficiently reduces the flow energy content within the entire span of the boundary layer. The estimated far-field trailing edge noise is reduced in the range of frequencies between 200 Hz and 1-2 kHz, with the highest levels of estimated noise reduction obtained at an angle of flow suction of $\alpha = 70^\circ$, at a suction rate high enough to achieve laminarisation.

I. Introduction

Over the last decades, researches have shown[1,2] that the sound generated by the interaction between turbulent flow and aerofoils represents one of the main contributors to the overall noise emissions from airplanes' wings, turbomachines, and wind farms. It is understood that trailing edge (TE) noise, in particular, is a dominant noise component.

The physical understanding of TE noise and its modelling have been the object of several investigations, with the ultimate goal of developing techniques for its attenuation. It was shown that as the hydrodynamic pressure field associated with the turbulent boundary layer passes over the trailing edge, the pressure field scatters into sound in a dipole manner.[1,2] Early investigations of trailing edge noise were limited to analytical modelling because the direct measurement of the far-field noise was not technically possible.[3–5] The majority of these models simplify the problem to a semi-infinite flat plate, where a zero pressure gradient turbulent boundary layer (TBL) is considered over the surface.[3,4,6–8] Amiet's trailing edge noise model[3,4] has become one of the most common methods to predict the trailing edge noise. Amiet considered the surface pressure fluctuations at the trailing edge as an acoustic source to estimate the far-field noise. The pioneering experimental work of Brooks and Hodgson[2] confirmed the accuracy of Amiet's predictions. Moreover,

*Research Associate, Kevin T. Crofton Department of Aerospace and Ocean Engineering, Virginia Tech
†Lecturer, Faculty of Engineering, University of Bristol
‡Reader, Faculty of Engineering, University of Bristol

Brooks, Pope & Marcolini[1] carried out an extensive study of far-field noise radiated by a NACA0012 aerofoil, and additionally, they provided a semi-empirical model (BPM model) for trailing edge noise. More recently, computational fluid dynamics (CFD) and large-eddy simulations (LES) were used to predict the far-field noise in a number of studies.[9–12] However, due to the complexity of the problem, mainly associated with the high Reynolds numbers, the numerical estimation of far-field trailing edge noise still remains computationally unfeasible.

In general, two sets of strategies exist that can lead to the attenuation of the far-field noise. On the one hand, changes introduced to the geometry of the trailing edge (i.e. the scattering condition) can be classified as *passive* noise reduction techniques. Examples of passive methods are the trailing edge serrations,[13–16,16–21] trailing edge brushes,[22,23] porous materials,[5,24–32] surface treatments,[33–36] shape optimization and morphing.[37] On the other hand, *active techniques* introduce changes to the boundary layer flow, which can reduce the energy content of the hydrodynamic pressure field and, therefore, they can reduce the trailing edge noise. The present work focuses on the use of flow suction to reduce the trailing edge noise. Uniform suction is applied in this work in an open-loop control approach, where the speed of the flow suction is varied independently of the emitted far-field noise or the freestream flow speed.

Understanding the effects of flow suction on the turbulent boundary layer is essential to utilize it efficiently as a noise control technique. In their pioneering study, Antonia *et al.*[38] observed that flow suction increases the stability of the longitudinal coherence of the large-scale low-speed streaks. Their dye flow visualizations revealed that suction reduces the average frequency of dye ejections from the wall into the outer region of the turbulent boundary layer. This effect is an indication of reduced turbulent activity within the boundary layer. Their work was followed by a series of experimental investigations on the effect of concentrated flow suction from a turbulent boundary layer at low Reynolds numbers, see Antonia *et al.*[39] and Oyewola *et al.*[40–42] The authors applied a wide range of suction rates (σ), which they defined as the ratio of momentum flux of flow suction and momentum flux of the boundary layer. Later, several studies on the effects of flow suction on a turbulent boundary layer reported that downstream of the flow control section the turbulent flow shows laminar behavior.[39–43] The streamwise length of the plate in the aforementioned experimental campaigns was sufficient to enable the flow recovery downstream of flow suction. At a suction rate of $\sigma = 2.6$, the boundary layer required a streamwise distance of $20\delta_0$, where δ_0 is the thickness of the undisturbed boundary layer, to recover its original state. This indicates that flow suction has a stable and long-lasting effect on the turbulent boundary layer.

As the main consequence of flow laminarisation, the turbulent energy content of the boundary layer was also observed to significantly decrease.[44] It can be expected that a boundary layer characterized with a lower turbulent energy content will impose lower amplitudes of pressure fluctuations on the wall. According to Amiet's model,[4] a reduction of the surface pressure fluctuations attenuates the predicted trailing edge noise. Therefore, the observed reduction of the energy content within the boundary layer makes flow suction a promising candidate for aeroacoustic purposes.

Flow suction was proven to be effective in reducing the trailing edge noise, see Wolf *et al.*,[45] Lutz *et al.*,[46] Matera[47] and Arnold *et al.*[48,49] However, the number of studies available is rather limited and they lack of in-depth flow analysis. Wolf *et al.*[45] conducted experiments to understand the effects of flow suction on trailing edge noise. They installed an area of flow suction consisting of four chambers positioned upstream of a NACA 643-418 aerofoil's trailing edge. The applied flow control severity was kept constant, while flow suction was applied further upstream of the trailing edge and closer to the trailing edge to study the effects of the location of flow suction. Their study lacks of the direct measurement of far-field noise, but they used an indirect noise measurement technique, which relies on hot-wire anemometry (Coherent Particle Velocimetry[50]) to predict the broadband far-field noise. The mean and root mean square (rms) velocity results were obtained immediately downstream (1 mm) of the blade. The velocity results indicate that the suction reduces the velocity deficit in the flow, and it significantly reduces the turbulent energy content within the boundary layer. They reported a reduction of up to 5 dB in the predicted far-field noise below 3 kHz, with some penalties observed at high frequencies (3-5 kHz). The study presented by Wolf *et al.*[45] is limited to the measurement of the mean and rms velocity profiles, which fails to explain the hydrodynamic effects of flow suction within the turbulent boundary layer. Lutz *et al.*[46] performed Reynolds averaged Navier-Stokes (RANS) simulations using the geometry of the same NACA 643-418 aerofoil as Wolf *et al.*[45] The results of the RANS simulations match the mean and rms velocity results presented by Wolf *et al.*[45]

In the present work, the effects of flow suction on a turbulent boundary layer are experimentally investigated. Flow suction is applied at four different suction angles ($\alpha = 30°, 50°, 70°$ and $90°$), which is defined

as the angle between the free-stream flow and flow suction velocity. In addition, a wide range of flow control severities (σ) are considered. The far-field trailing edge noise is estimated with Amiet's model,[4] using the signals of the surface pressure fluctuations acquired from flush-mounted microphones.

II. Experimental Approach

Figure 1 gives the geometrical description of the rig and provides the definition of the coordinate system. The coordinate system consists of streamwise (x), wall normal (y), and spanwise (z) directions, and its origin is at the mid-span of the plate, at the downstream edge of the active flow control section. The flow control section is located between 120 mm and 150 mm upstream of the trailing edge. The flow suction method consists of two main parts: a honeycomb structure and, on top of it, a wire mesh. The honeycomb structure is 10 mm thick, and its pores are inclined upstream with respect to the free-stream flow to ease the entry of the boundary layer flow into the flow control section, see Fig. 1(b). The inclination of the honeycomb pores defines the flow control angle, α. In the current work, four different flow control angles are considered, namely $\alpha = 30°, 50°, 70°$, and $90°$. The length of the flow control section is $b = 30$ mm for all cases of flow suction angles. Air was drawn from the flow control section by using a radial fan, which was controlled within a Matlab environment. The power of the fan was finely adjustable, ensuring the repeatability of the applied flow suction severity.

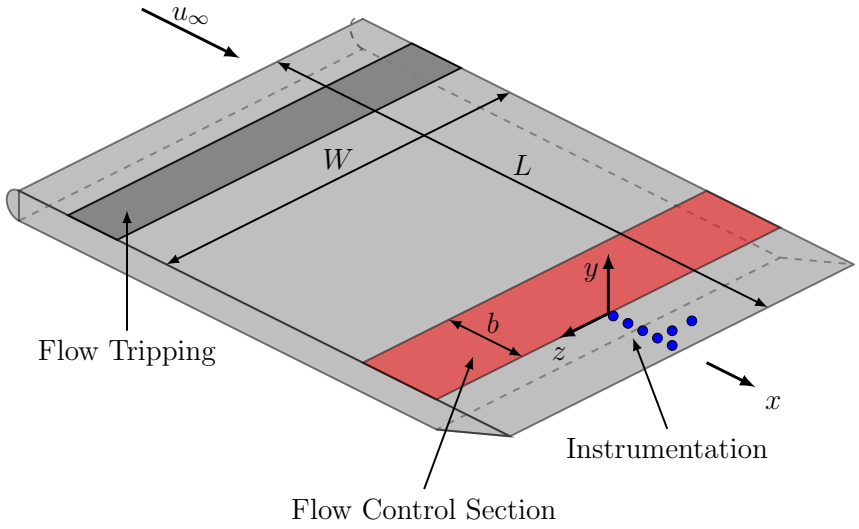

(a) Schematics of the rig.

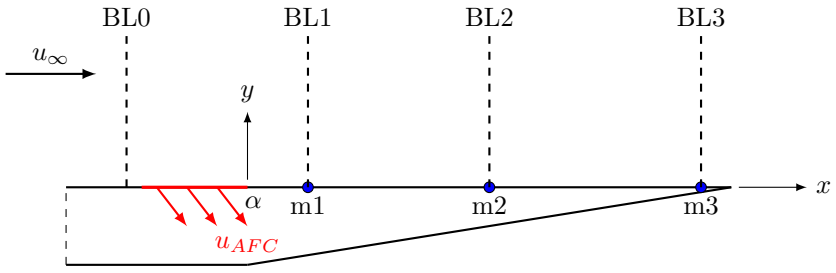

(b) Schematics of the hot-wire measurements.

Figure 1. Schematics of the rig (a) and the simultaneous hot-wire measurements (b) performed at locations BL0, BL1, BL2 and BL3, corresponding to $x/\delta_0 = -1, 0.6, 1.8$ and 4, respectively.

Flush-mounted FG-23329-P07 type Knowles electret condenser microphones were used for the measurement of unsteady surface pressure fluctuations. A total number of 21 transducers were distributed both in the streamwise and spanwise directions close to the trailing edge, as shown in Fig. 1(a). The miniature microphones were calibrated prior to the measurements, and their uncertainty was found to be ± 0.5 dB within

the investigated frequency range assuming a normal distribution of pressure fluctuations.[51] The microphones were mounted below a pinhole with a diameter of $d = 0.4$ mm. The attenuation of the pressure signal can be considered negligible, should the dimensionless pinhole diameter ($d^+ = du_\tau/\nu$) be below $d^+ = 19$ (see Schewe[52]). The current configuration resulted in $d^+ \approx 17$, therefore the pressure attenuation introduced by the pinhole was found to be negligible. In addition, the discontinuity on the surface does not have any significant influence on the boundary layer.

Dantec 55P16 type single-sensor hot-wire probes were used to measure the turbulence statistics of the flow velocity over the entire boundary layer (along the y axis) at axial locations BL0, BL1, BL2, and BL3. The probes were operated by a Dantec StreamWare Pro CTA91C10 module, at an overheat ratio of 1.8. The uncertainty of the measured velocity was found to be less than 0.5 % over the entire range of investigated velocities. The data were acquired simultaneously from the flush-mounted microphones and the hot-wire sensor using a National Instruments PXIe-4499 system, at a sampling rate of f_s =65,536 Hz (= 2^{16} Hz), for a time span of 16 seconds.

Data processing was performed with the use of Python's SciPy package. When calculating spectra and coherence, a digital filter was applied in order to reduce low-frequency measurement noise.[53] Time signals were divided into smaller segments with a 50 % overlapping. The length of the time segments (WS) was defined such that the frequency resolution ($\Delta f = 4f_s/WS$) of the transformed signal was $\Delta f = 64$ Hz. Hamming windowing was then applied to each segment, which was followed by the calculation of their fast Fourier transform (FFT). After the Fourier transform of each segment, the energy loss in the signal caused by the application of Hamming windowing was compensated, and the FFT results were averaged to achieve a smooth resolution of spectra in the frequency domain.

Two different sets of measurements were performed, which are depicted in Fig. 1(b). In the first set of measurements, signals from all flush-mounted microphones were simultaneously recorded for a wide range of flow suction velocities ($u_{AFC} = 0.2 - 0.9u_\infty$) and flow control angles ($\alpha = 30°, 50°, 70°$ and $90°$). During the second set of measurements, the streamwise velocity was measured with hot-wire anemometry along the entire wall-normal span of the turbulent boundary layer thickness, at four different streamwise locations, marked as BL0, BL1, BL2 and BL3 (see the dashed lines in Fig. 1(b)). The streamwise locations of BL0, BL1, BL2 and BL3 are listed in Table 1. At BL1, BL2, and BL3, the streamwise velocity and surface pressure fluctuations using microphones marked by m1, m2 and m3 in Fig. 1(b) were recorded simultaneously.

	BL0	BL1 (m1)	BL2 (m2)	BL3 (m3)
x/δ_0 (-)	-1.0	0.6	1.8	4.0

Table 1. Locations of the simultaneous velocity and surface pressure measurements.

The flow control severity, σ, relates the momentum deficit of the boundary layer to the momentum of the flow control system. According to Antonia *et al.*,[39] the *flow control severity* (σ) can be quantified as follows:

$$\sigma = \frac{u_{AFC} b}{u_\infty \theta_0}, \tag{1}$$

where u_{AFC} is the magnitude of the flow suction velocity, $b = 30$ mm is length of the flow control section, $u_\infty = 15$ m/s is the velocity of the free-stream flow, and $\theta_0 = 2.6$ mm is the momentum thickness of the non-disturbed boundary layer. In the current work, three values of flow control severity (σ) are considered for each flow control angle (α), namely, $\sigma = 0$ (baseline case), a lower σ and a higher σ. The parameters of the applied flow control cases (i.e. α and σ values) and the corresponding boundary layer properties are listed in Table 2.

III. Boundary Layer Development

Based on the two sets of measurements described in Section II, the effects of flow suction on the turbulent boundary layer are firstly examined in this section, followed by its effects on the estimated far-field noise. In order to understand the effects of uniform flow suction on the turbulent boundary layer, the developing flow pattern is firstly investigated by means of turbulent statistics obtained at locations BL0, BL1, BL2 and BL3, see Fig. 1(b).

σ	δ [mm]			δ^* [mm]			θ [mm]			u_τ [m/s]		
	BL1	BL2	BL3	BL1	BL2	BL3	BL1	BL2	BL3	BL1	BL2	BL3
0	29	30	30	3.81	3.71	3.69	2.59	2.63	2.57	0.617	0.618	0.657
						$\alpha = 30°$						
2.5	57	46	15	3.69	2.70	1.20	3.08	2.21	2.01	0.692	0.679	0.587
3.7	58	49	10	3.84	2.42	1.30	3.23	1.98	1.12	0.596	0.623	0.612
						$\alpha = 50°$						
4.3	55	45	16	3.24	1.93	1.05	2.86	1.75	0.85	0.769	0.616	0.818
6.2	62	48	5	3.83	1.94	0.55	3.40	1.72	0.35	0.705	0.660	0.672
						$\alpha = 70°$						
5.0	60	54	3	3.76	2.58	0.25	3.34	2.14	0.17	0.797	0.616	0.858
7.5	63	61	1	4.69	3.21	0.31	4.11	2.65	0.15	0.524	0.558	0.787
						$\alpha = 90°$						
6.1	65	56	4	4.53	2.78	0.42	3.87	2.44	0.22	0.603	0.772	0.748
9.1	58	49	1	5.69	3.25	0.50	4.79	2.83	0.18	0.523	0.588	0.600

Table 2. Boundary layer properties measured for the different flow control angles ($\alpha = 30°, 50°, 70°$ and $90°$) at locations BL1, BL2 and BL3, corresponding to $x/\delta_0 = 0.6, 1.8$ and 4, respectively.

A. Mean Velocity Profiles

In order to investigate the evolution of the boundary layer along the wall-normal direction, the streamwise velocity was measured at BL0, BL1, BL2, and BL3, corresponding to $x/\delta_0 = -1, 0.6.1.8$ and 4, respectively. The mean velocity results obtained from these hot-wire measurements are presented in Fig. 2, at locations BL0, BL1, BL2, and BL3, for $\alpha = 30°, 50°, 70°$ and $90°$. Additional boundary layer parameters, such as boundary layer thickness (δ), displacement thickness (δ^*), momentum thickness (θ) and friction velocity (u_τ) are presented in Table 2 for varying α and σ at locations BL1, BL2 and BL3. From the velocity profiles shown in Fig. 2, we can observe that the flow suction affects the entire boundary layer both upstream (BL0) and downstream (BL1-BL3) of the flow control treatment. At BL0, the mean velocity profiles in Fig. 2 reveal that the flow is accelerated as a result of flow suction. The amount of increase in the velocity profiles at BL0 increases with increasing flow control severity (σ) and with flow suction angle (α). These findings are consistent with the results of Antonia *et al.*[39]

At BL1 ($x/\delta_0 = 0.6$), the boundary layer profiles indicate a momentum deficit at $y > 0.4\delta_0$ for the flow suction cases ($\sigma > 0$) compared to the baseline boundary layer ($\sigma = 0$). Based on the definition of the boundary layer thickness (δ) as $\bar{u}(\delta) = 0.99u_\infty$, δ increases at BL1 in consequence of flow suction, as a result of the observed momentum deficit at $y > 0.4\delta_0$. In agreement with this, the boundary layer integral parameters (δ^*, θ) also increase at BL1 as an effect of flow suction (see Table 2). The DNS simulations of Park and Choi[44] revealed that the increase of boundary layer parameters, such as δ, δ^*, and θ is due to the momentum deficit caused by the extracted fluid at the flow control section. Below $y = 0.4\delta_0$, the mean velocity exceeds the values of the baseline case. At BL2, the boundary layer profiles are very similar to those at BL1, but the crossing point above which a decrease in $\bar{u}$ (i.e. momentum deficit) is observed takes place at larger wall-normal locations, i.e. at $y \approx 0.7\delta_0$. This observation suggests that the boundary layer flow is moving towards the plate. Additionally, the boundary layer thickness (δ) at BL2 grows at increasing σ,

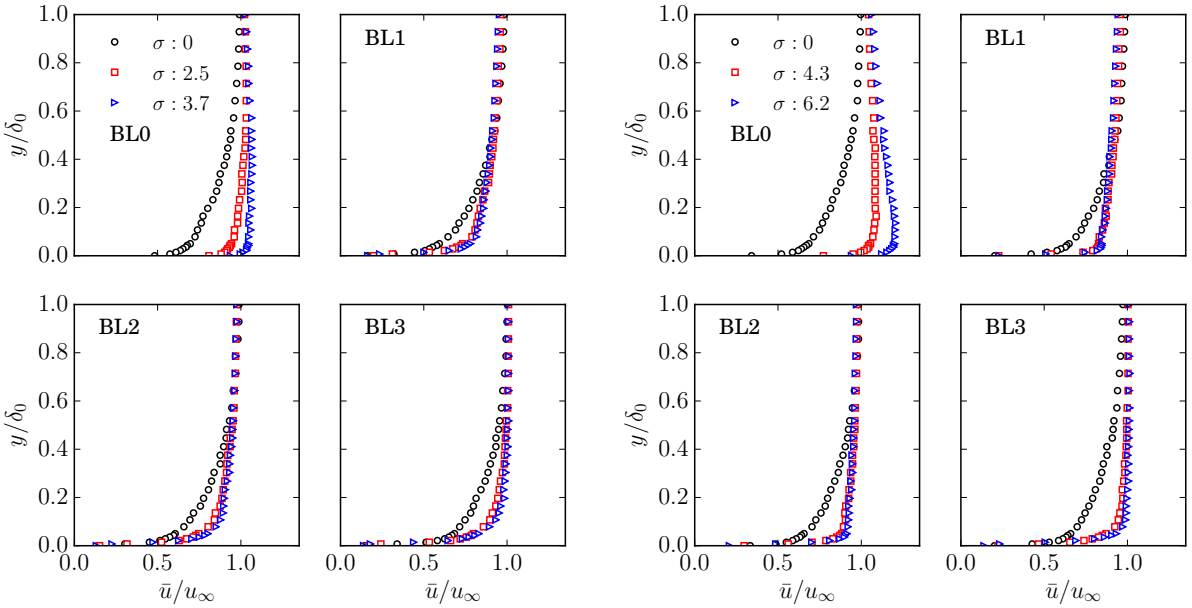

(a) $\alpha = 30°$ flow control angle.

(b) $\alpha = 50°$ flow control angle.

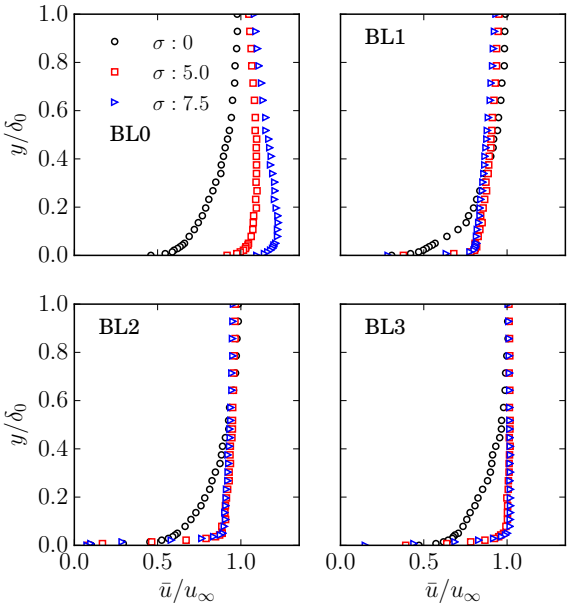

(c) $\alpha = 70°$ flow control angle.

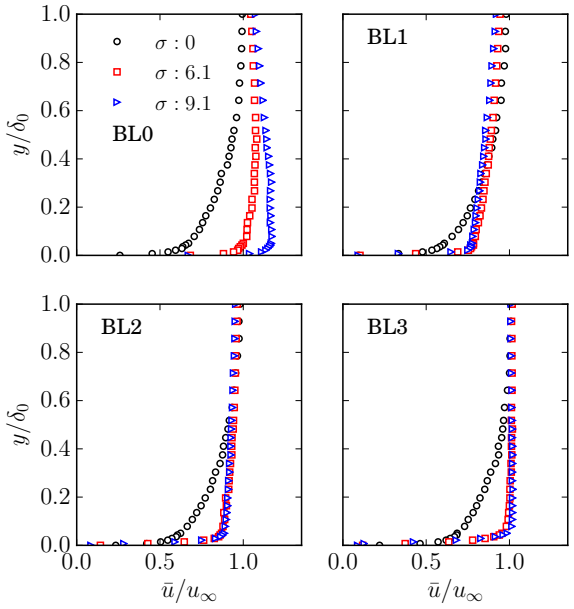

(d) $\alpha = 90°$ flow control angle.

Figure 2. Mean velocity profiles measured at flow control angles (a) $\alpha = 30°$, (b) $\alpha = 50°$, (c) $\alpha = 70°$ and (d) $\alpha = 90°$ at locations BL0, BL1, BL2 and BL3.

independent of the flow control angle α. An exception to this is observed for $\alpha = 90°$, where the boundary layer thickness is found to decrease for $\sigma = 9.1$ with respect to $\sigma = 6.1$, see Table 2. In the vicinity of the trailing edge, at BL3, the boundary layer profiles for $\sigma > 0$ are different from the boundary layer profiles observed at BL1 and BL2. The main boundary layer parameters, such as the boundary layer thickness (δ), displacement thickness (δ^*) and momentum thickness (θ) are observed to significantly decrease at BL3 as compared to the upstream locations of BL1 and BL2, independent of flow control angle (α) and severity (σ). In particular, the higher the flow control angle (α) and flow suction severity (σ), the higher is the reduction of δ, δ^*, and θ. However, δ^* and θ are observed to increase when moving from $\alpha = 70°$ to $\alpha = 90°$. This suggests that the perpendicular flow suction loses efficiency with respect to $\alpha < 90°$. In general, if the free-stream velocity is reached over shorter wall-normal distance than for the baseline case ($\sigma = 0$), the mean shear within the boundary layer ($\mathrm{d}u/\mathrm{d}y$) increases. This observation was also reported by Park and Choi[44] who showed that immediately downstream of the flow suction area, the skin friction coefficient increases as a consequence of flow suction. Finally, from the observation of the mean velocity profiles in Fig. 2, it seems that the use of flow suction does not result in boundary layer separation, which suggests that the aerodynamic behavior of the flat plate is not significantly affected. However, wind tunnel measurements with a force balance should be performed to quantify possible changes in lift and drag.

B. Dimensionless Velocity Profiles

Dimensionless velocity profiles are shown in Figs. 3 and 4, for $\alpha = 30°, 50°$ and $\alpha = 70°, 90°$, respectively. The $+$ superscript denotes normalisation by inner boundary layer quantities, i.e. $u^+ = \bar{u}/u_\tau$ and $y^+ = yu_\tau/\nu$. As noticed from the observation of the mean velocity profiles ($\bar{u}$) in Fig. 2, suction affects the mean velocity within the boundary layer over its entire span. As a result, the structure of the boundary layer is expected to change as well. The effects of the flow suction on the turbulent boundary layer structure can be appreciated when observing the dimensionless velocity profiles in Figs. 3 and 4. The different portions of the boundary layer are identified for the baseline case ($\sigma = 0$) with the help of the Spalding's equation,[54] which is presented by black dashed lines in Figs. 3 and 4. As can be seen from Figs. 3 and 4, a portion of the buffer layer is resolved below $y^+ < 20$ ($y/\delta_0 < 0.05$). The logarithmic region is located between $20 < y^+ < 300$ ($0.05 < y/\delta_0 < 0.2$), followed by the wake layer $300 < y^+ < 2000$ ($0.2 < y/\delta_0 < 1$), until the mean velocity reaches the value of the free-stream velocity. These boundary layer regions are in good agreement with the numerical data provided by Schlatter and Örlü[55] at a similar range of Reynolds number. Figures 3 and 4 reveal that the flow suction significantly affects the boundary layer structure downstream of the flow control section. At BL1 ($x/\delta_0 = 0.6$), for the most shallow flow suction angle ($\alpha = 30°$) and at the lowest suction severity ($\sigma = 2.5$) the buffer layer follows the properties of the baseline case. The lowest amount of flow suction ($\sigma = 2.5$) reduces the span of the logarithmic region at BL1 to the range of $20 < y^+ < 100$ approximately, see Fig. 3(a). Similar observations can be made in case of $\alpha = 30°$ for both σ rates at location BL2 ($x/\delta_0 = 1.8$). At BL3, on the other hand, the dimensionless velocity (u^+) deviates more from the baseline case compared to BL1 and BL2. A possible explanation for this can be that the presence of the trailing edge affects the boundary layer at BL3. Similar observations can be made at higher flow control angles (α) and flow suction severity (σ). At $\alpha = 50°, 70°$ and $90°$, the u^+ results follow the shape of the viscous region ($u^+ = y^+$) at low dimensionless wall distances ($y^+ < 10 - 20$). The larger extent of the viscous region indicates partial laminarisation at all streamwise locations under analysis. In addition, the results indicate that the wall-normal extent of the logarithmic region is significantly reduced. Therefore, it can be expected that the turbulence properties of the turbulent motions formerly located at the logarithmic region are also affected by flow suction. The results suggest that partial laminarisation is reached at $\sigma \approx 6$. Above $\sigma \approx 6$, the effects of flow control is preserved at further downstream locations of BL1, as the $u^+(y^+)$ profiles significantly depart from Spalding's equation at BL2 and BL3 in the case of $\alpha = 70°$ and $90°$. The present behaviour of the dimensionless velocity profiles agrees well with previous findings presented at similar streamwise locations (x/δ_0) by Oyewola *et al.*[42] and Antonia *et al.*[39]

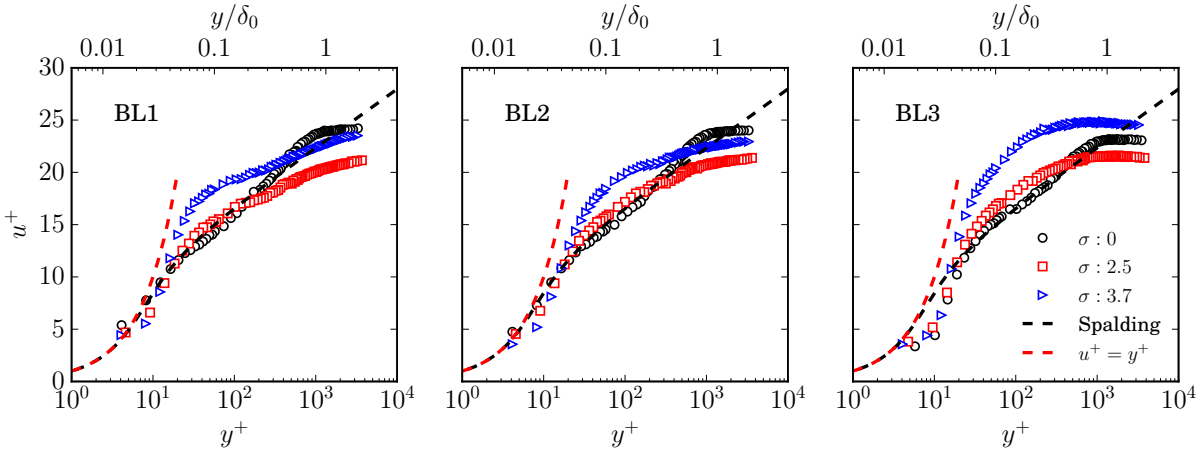

(a) $\alpha = 30°$ flow control angle.

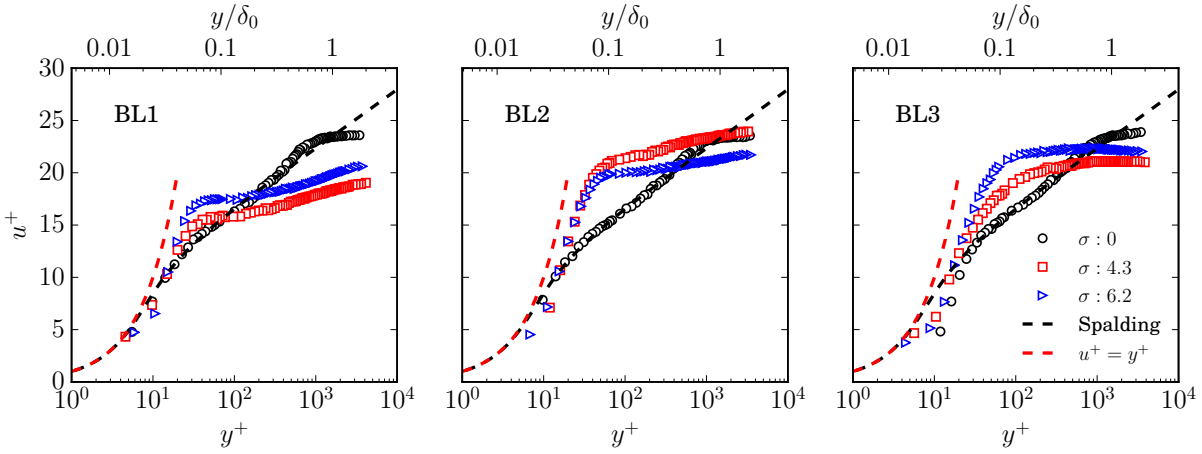

(b) $\alpha = 50°$ flow control angle.

Figure 3. Dimensionless velocity profiles at flow control angles (a) $\alpha = 30°$ and (b) $\alpha = 50°$ at locations BL1, BL2 and BL3.

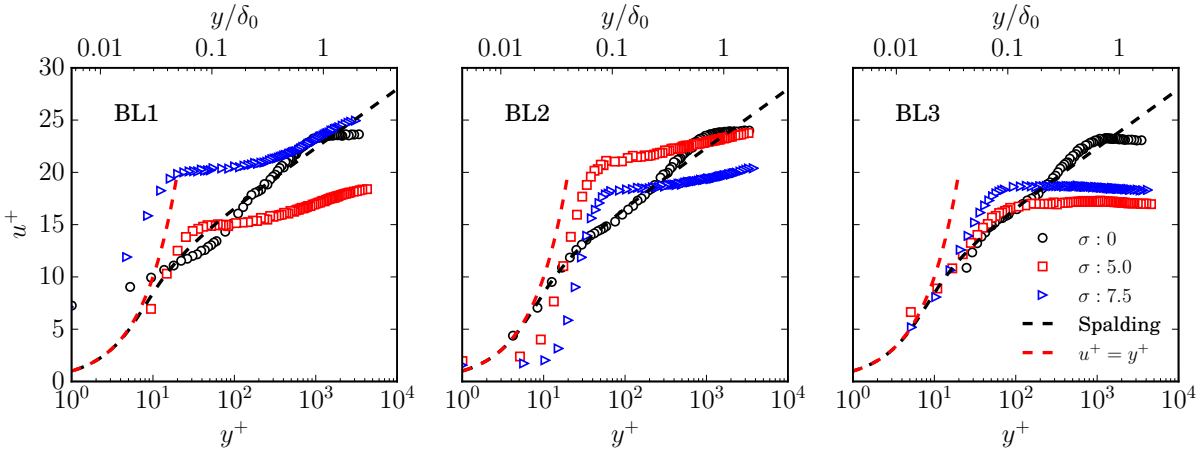

(a) $\alpha = 70°$ flow control angle.

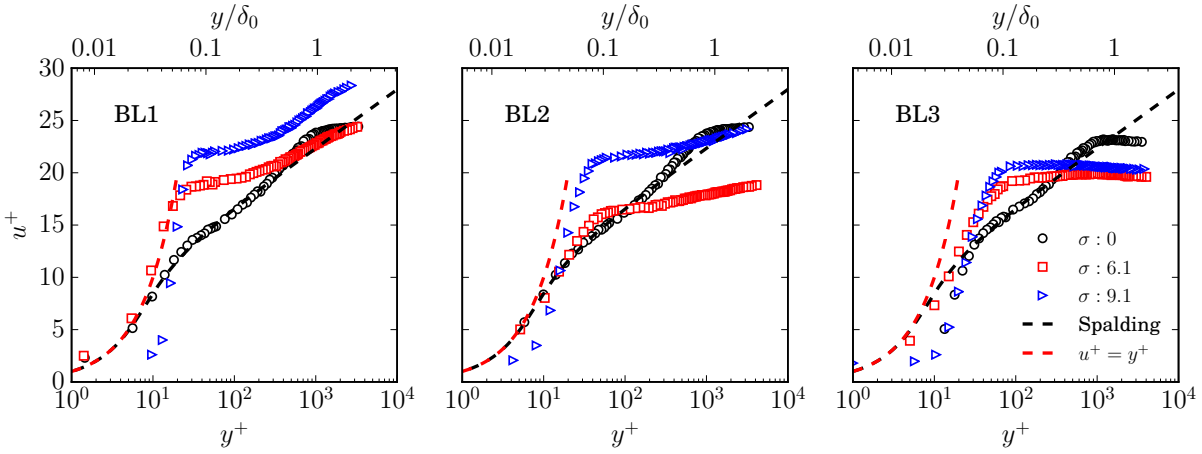

(b) $\alpha = 90°$ flow control angle.

Figure 4. Dimensionless velocity profiles at flow control angles (a) $\alpha = 70°$ and (b) $\alpha = 90°$ at locations BL1, BL2 and BL3.

C. Root Mean Square Velocity Profiles

The root mean square (rms) velocity results obtained from the hot-wire measurements are presented in Fig. 5, at BL0, BL1, BL2 and BL3, for $\alpha = 30°, 50°, 70°$ and $90°$, and for three values of flow suction severity. Similarly to the $\bar{u}$ results shown in Fig. 2, the rms results reveal that uniform flow suction affects the energy content of the entire turbulent boundary layer, therefore not only the near-wall region. At BL0, independent of the flow control angle α, flow suction has the effect of reducing the energy content over the entire boundary layer. The reduction of rms at BL0 grows with increasing flow suction severity. These observations indicate that, similarly to the increase in $\bar{u}$ formerly seen at location BL0 in Fig. 2, the flow is accelerated upstream of the flow control treatment. Downstream of the flow control treatment, i.e. at BL1-BL3, the energy content within the boundary layer is significantly lower over the entire extent of the boundary layer for all cases of α and σ as a consequence of flow suction. Therefore, flow suction is effective in removing turbulent kinetic energy from the boundary layer over the whole range of wall-normal locations. The underlying mechanism leading to the reduction of the energy content was investigated in previous computational and experimental studies. As reported in Refs.,[39–44] flow suction increases viscous diffusion, which was found to be responsible for the break-up of turbulent structures. As a result of this, flow suction was found to reduce the turbulence intensities and Reynolds shear stresses. The observed reduction of the energy content within the turbulent boundary layer is therefore in good agreement with previous studies.

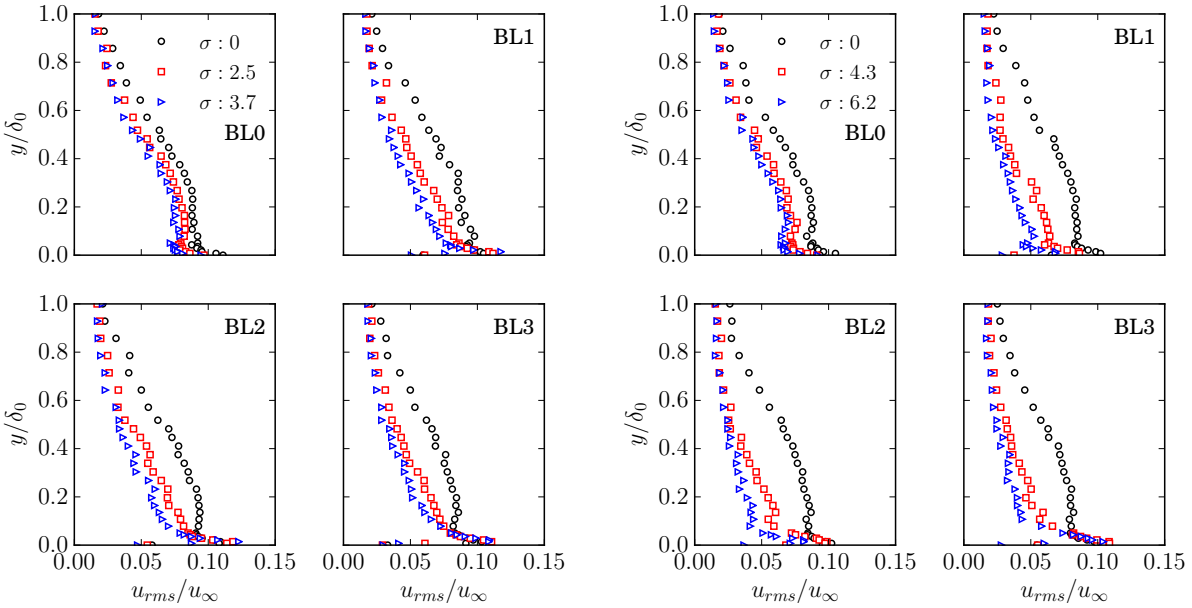

(a) $\alpha = 30°$ flow control angle.

(b) $\alpha = 50°$ flow control angle.

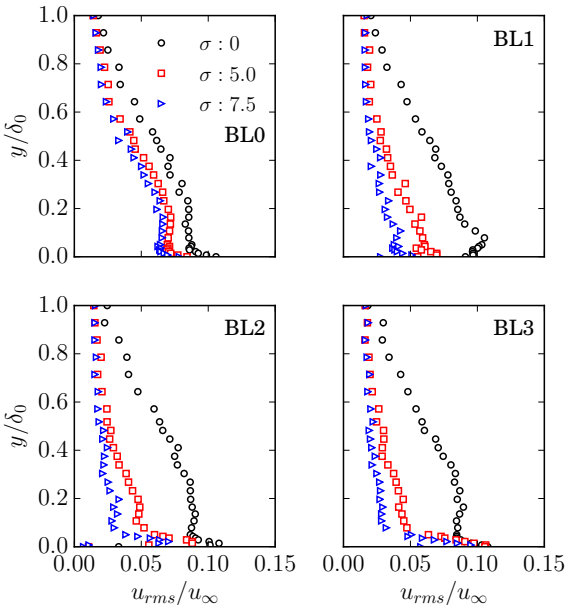

(c) $\alpha = 70°$ flow control angle.

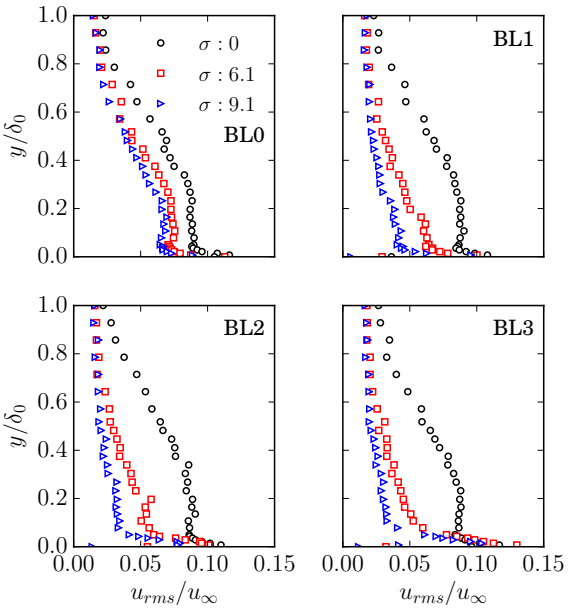

(d) $\alpha = 90°$ flow control angle.

Figure 5. Root mean square velocity profiles measured at flow control angles (a) $\alpha = 30°$, (b) $\alpha = 50°$, (c) $\alpha = 70°$ and (d) $\alpha = 90°$ at locations BL0, BL1, BL2 and BL3.

D. Estimates of Far-field Noise

Figure 6 presents the far-field noise (S_{pp}) estimated using Amiet's trailing edge noise model[4] with an observer located 1 m above the trailing edge for all considered cases of α and σ. According to Amiet's model, the product between the integral spanwise length scales of the turbulent structures (Λ_z) and the power spectrum of the surface pressure fluctuations (ϕ_{pp}) drives the generated far-field noise, therefore the reduction of this product determines the success of a noise attenuation method. In general, S_{pp} shows that flow suction reduces the far-field noise over a wide range of frequencies. The predicted far-field noise is observed to increase at low frequencies below $f = 200$ Hz. In the mid-frequency region, however, flow suction shows significant reductions in the far-field noise. For $\alpha = 30°$, the frequency band where a reduction is observed ranges between 200 Hz and 1-2 kHz. The extent of the frequency band where noise attenuation is obtained enlarges for increasing flow suction severity. On the other hand, the range of frequencies where the flow control technique fails remains invariably confined to frequencies lower than 200 Hz, independent of both the flow control severity (σ) and the angle (α). Therefore, the frequency range where a reduction of the estimated far-field noise is achieved increases with increasing σ. When comparing Fig. 6(c) and 6(d), i.e. flow suction at $\alpha = 70°$ and $\alpha = 90°$, it can be seen that flow suction at $\alpha = 70°$ is more efficient in reducing the far-field trailing edge noise than at $\alpha = 90°$, which is consistent with the profiles of u_{rms}. Additionally, the results related to a suction of 70° reveal that once laminarisation is achieved, further increases in the suction severity do not result in a more significant reduction of far-field noise. Laminarisation was observed for a flow control severity of $\sigma \approx 6$.

The far-field noise was also calculated with an observer located at 1 m radius from the trailing edge with varying polar angles of $0° - 180°$. The far-field noise overall sound pressure level (OASPL, dB) was calculated by integrating S_{pp} over the frequency range of $100 - 10,000$ Hz. Results are shown in Fig. 7, at different polar angles. In general, a reduction of OASPL is observed when flow suction is applied ($\sigma > 0$). This indicates that the observed increase of the estimated far-field noise at low frequencies (see Fig. 6) is less dominant than the broadband reduction at mid-frequencies. In agreement with S_{pp}, as the flow suction severity (σ) and flow control angle (α) grow, the OASPL undergoes a decrease. Also, in agreement with the previous results, $\alpha = 70°$ exhibits the best performance in reducing the OASPL levels, and a noise reduction up to 5 dB is estimated at $\sigma > 6$. Once partial laminarisation is reached ($\sigma \approx 6$), further increasing σ does not provide any additional reductions of the estimated far-field noise. Therefore, based on the results shown in the present work, applying uniform flow suction at a flow control angle $\alpha = 70°$ with a flow control severity $\sigma \approx 6$ seems to offer the best performances in terms of attenuation of the estimated far-field trailing edge noise, at the highest efficiency.

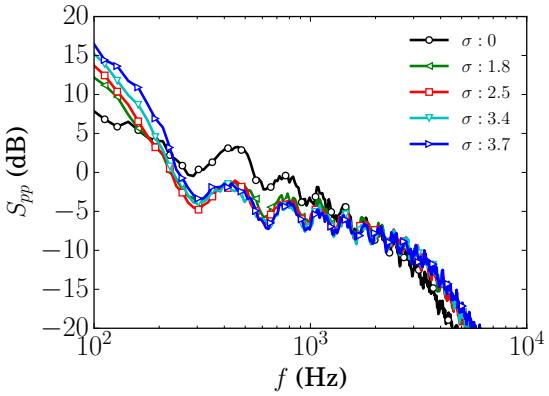

(a) $\alpha = 30°$ flow control angle.

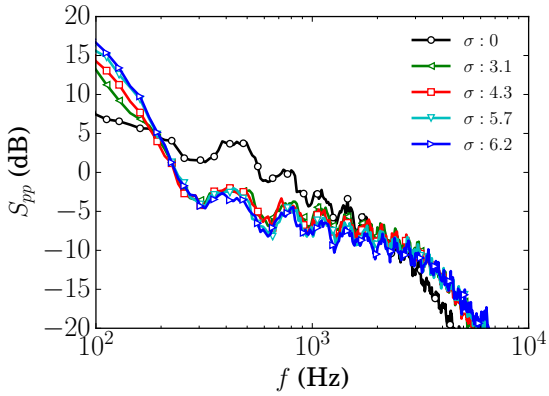

(b) $\alpha = 50°$ flow control angle.

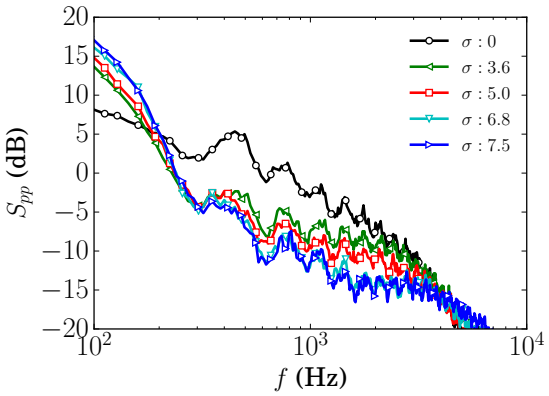

(c) $\alpha = 70°$ flow control angle.

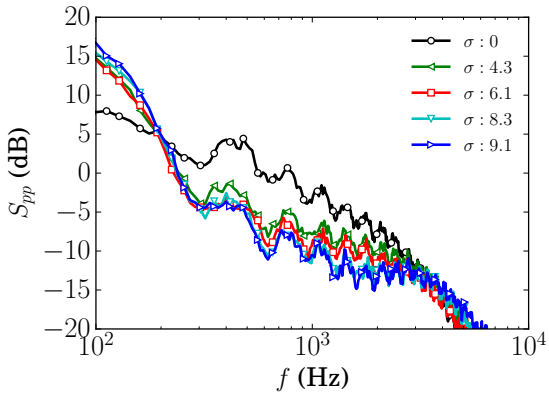

(d) $\alpha = 90°$ flow control angle.

Figure 6. Estimation of far-field noise at flow control angles (a) $\alpha = 30°$, (b) $\alpha = 50°$, (c) $\alpha = 70°$ and (b) $\alpha = 90°$ using Amiet's trailing edge noise model with the observer located at a vertical distance of 1 m above the trailing edge.

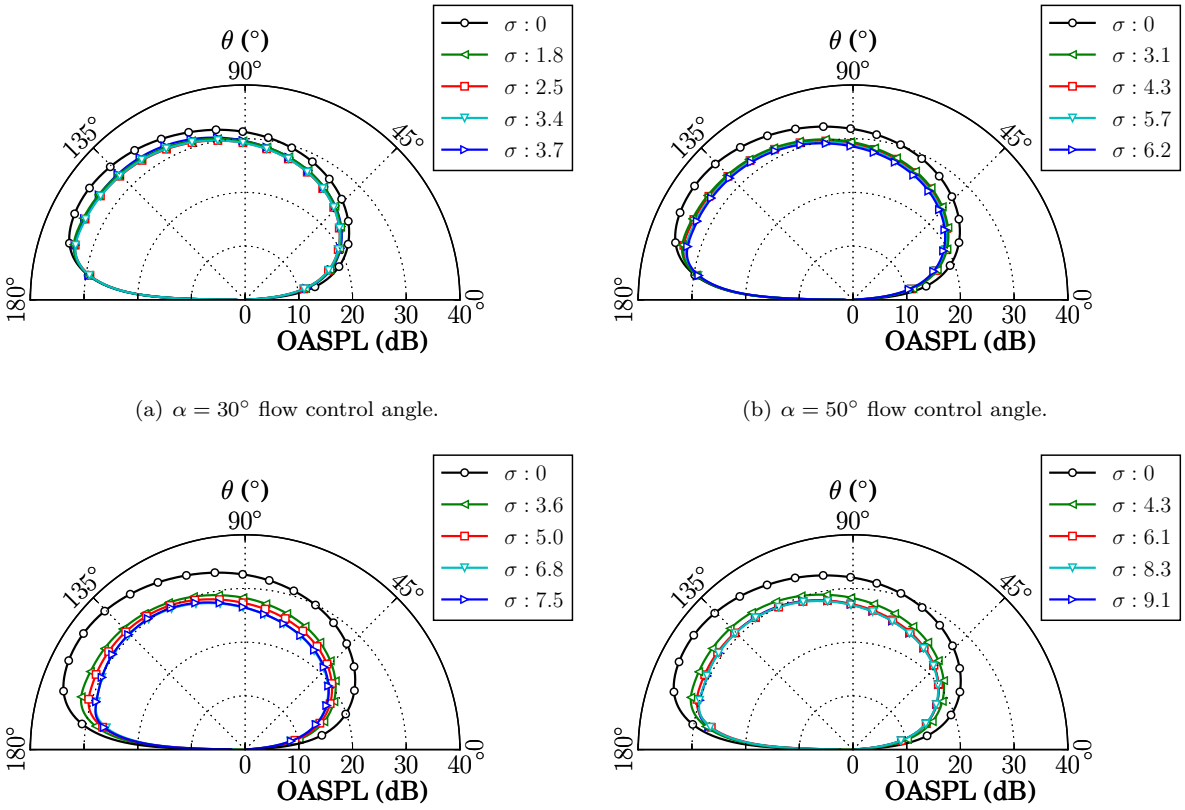

(a) $\alpha = 30°$ flow control angle.

(b) $\alpha = 50°$ flow control angle.

(c) $\alpha = 70°$ flow control angle.

(d) $\alpha = 90°$ flow control angle.

Figure 7. Estimation of far-field noise overall sound pressure level at flow control angles (a) $\alpha = 30°$, (b) $\alpha = 50°$, (c) $\alpha = 70°$ and (b) $\alpha = 90°$ using Amiet's trailing edge noise model with the observer located at different polar angles with a radial distance of 1 m above the trailing edge.

IV. Conclusions

The present work investigated the use of uniform flow suction for the reduction of trailing edge noise. The flow control treatment was installed on the flat plate rig upstream of a trailing edge, with the aim of controlling the hydrodynamic pressure field associated with the turbulent boundary layer. Simultaneous measurements of streamwise velocity with hot-wire anemometry, and surface pressure fluctuations using flush-mounted microphones were performed at a number of locations downstream of the active flow control treatment. Data were collected at different flow control angles ($\alpha = 30°, 50°, 70°$ and $90°$), which is the angle of flow suction with respect to the free-stream flow, and at a range of flow control severities (or rates of flow suction) $\sigma = u_{AFC}b/u_\infty\Theta = [1.8, 9.1]$.

The main large-scale parameters of the turbulent boundary layer, i.e. boundary layer thickness (δ), displacement thickness (δ^*), momentum thickness (θ), were found to increase in consequence of flow suction, consistent with the simulations of Park and Choi.[44] In particular, these parameters tend to grow for increasing suction rate σ and angle of suction α. The non-dimensional mean velocity profiles revealed that the wall-normal extent of the viscous region increases in consequence of flow suction, while the logarithmic region tends to reduce in size at growing suction rates. At suction rates larger than $\sigma > 6$, the logarithmic region disappears, which is evidence for a tendency towards flow laminarisation. This observation was in fair agreement with the experiments of Oyewola *et al.*,[42] who reported laminarisation above $\sigma = 5.5$. Consistent with these evidences of laminarisation, the flow energy content was also observed to significantly decrease.

The estimation of far-field trailing edge noise using Amiet's model[4] showed that inclined uniform suction resulted in the reduction of the radiated noise over a wide range of frequencies. The extent of the frequency band where noise attenuation was obtained enlarges for increasing flow suction severity. The largest amount of reduction in the estimated far-field noise was found in the range of frequencies between 200 Hz and 1-2 kHz, and it was obtained at an angle of flow suction of $\alpha = 70°$, for suction rates $\sigma > 6$. The results related to a suction of $70°$ revealed also that once laminarisation is achieved, further increases in the suction severity do not result in a more significant reduction of far-field noise. At frequencies lower than $f = 200$ Hz, the associated far-field noise increases significantly. From integrating the estimated far-field noise over the frequency range of $100 - 10,000$ Hz, we obtained the far-field noise overall sound pressure level, OASPL, at different polar angles. In general, a reduction in the OASPL was observed when flow suction was applied ($\sigma > 0$). In agreement with the estimated trailing edge noise, the OASPL undergoes a decrease for increasing flow suction severity (σ) and for growing suction angle (α). Flow suction at an angle of $\alpha = 70°$ and at $\sigma > 6$ was found to exhibit the best performance in reducing the OASPL levels, with a consequent noise reduction of up to 5 dB.

References

[1]Brooks, T. F., Pope, D. S., and Marcolini, M. A., "Airfoil Self-Noise and Prediction," *NASA Report*, Vol. 1218, 1989.

[2]Brooks, T. F. and Hodgson, T. H., "Trailing Edge Noise Prediction from Measured Surface Pressures," *Journal of Sound and Vibration*, Vol. 78(1), 1981, pp. 69–117.

[3]Amiet, R. K., "Acoustic radiation from an airfoil in a turbulent stream," *Journal of Sound and Vibration*, Vol. 41, No. 4, 1975, pp. 407–420.

[4]Amiet, R. K., "Noise Due to Turbulent Flow Past a Trailing Edge," *Journal of Sound and Vibration*, Vol. 47(3), 1976, pp. 387–393.

[5]Howe, M., "On the Added Mass of a Perforated Shell, with Application to the Generation of Aerodynamic Sound by a Perforated Trailing Edge," *Proceedings of the Royal Society of London. Series A, Mathematical and Physical Sciences*, Vol. 365, No. 1721, 1979, pp. 209–233.

[6]Ffowcs-Williams, J. E. and Hawkings, D. L., "Sound Generation by Turbulence and Surfaces in Arbitrary Motion," *Philosopical Transactions of the Royal Society London*, Vol. 264, 1969, pp. 321–342.

[7]Ffowcs-Williams, J. E. and Hall, L. H., "Aerodynamic sound generation by turbulent flow and in the vicinity of a scattering half plane," *Journal of Fluid Mechanics*, Vol. 40(4), 1970, pp. 657–670.

[8]Chase, D. M., "Noise radiated from an edge in turbulent flow," *AIAA Journal*, Vol. 13, No. 8, 1975, pp. 1041–1047.

[9]Wang, M., "Computation of trailing-edge noise at low Mach number using LES and acoustic analogy," *Centre for Turbulence Research, Annual Research Briefs*, 1998, pp. 91–105.

[10]Wang, M. and Moin, P., "Computation of trailing-edge flow and noise using large-eddy simulation," *AIAA Journal*, Vol. 38, No. 12, 2000, pp. 2201–2209.

[11]Ewert, R. and Schroeder, W., "On the simulation of trailing edge noise with a hybrid LES/APE method," *Journal of Sound and Vibration*, Vol. 270, No. 3, 2004, pp. 509 – 524.

[12]Wolf, W. R. and Lele, S. K., "Trailing-Edge Noise Predictions Using Compressible Large-Eddy Simulation and Acoustic Analogy," *AIAA Journal*, Vol. 50(11), 2012.

[13]Lyu, B., Azarpeyvand, M., and Sinayoko, S., "Prediction of noise from serrated trailing edges," *Journal of Fluid Mechanics*, Vol. 793, 2016, pp. 556–588.

[14]Liu, X., Showkat Ali, S. A., and Azarpeyvand, M., "On the Application of Trailing-edge Serrations for Noise Control from Tandem Airfoil Configurations," *23rd AIAA/CEAS Aeroacoustics Conference*, 2017, p. 3716.

[15]Pang, E., Cambray, A., Rezgui, D., Azarpeyvand, M., and Showkat Ali, S. A., "Investigation Towards a Better Understanding of Noise Generation from UAV Propellers," *2018 AIAA/CEAS Aeroacoustics Conference*, 2018, p. 3450.

[16]Gruber, M., Joseph, P., and Azarpeyvand, M., "An experimental investigation of novel trailing edge geometries on airfoil trailing edge noise reduction," *19th AIAA/CEAS Aeroacoustics Conference*, AIAA-2013-2011.

[17]Liu, X., Kamliya, H. J., Azarpeyvand, M., and Theunissen, R., "Wake Development of Airfoils with Serrated Trailing Edges," *22nd AIAA/CEAS Aeroacoustics Conference*, AIAA-2016-2817.

[18]Chong, T., Vathylakis, A., Joseph, P., and Gruber, M., "Self-Noise Produced by an Airfoil with Nonflat Plate Trailing-Edge Serrations," *AIAA Journal*, Vol. 51, No. 11, 2013, pp. 2665–2677.

[19]Chong, T. and Joseph, P., "An experimental study of airfoil instability tonal noise with trailing edge serrations," *Journal of Sound and Vibration*, Vol. 332, No. 24, 2013, pp. 6335–6358.

[20]Chong, T., Joseph, P., and Gruber, M., "Airfoil self noise reduction by non-flat plate type trailing edge serrations," *Applied Acoustics*, Vol. 74, No. 4, 2013, pp. 607–613.

[21]Azarpeyvand, M., Gruber, M., and Joseph, P., "An analytical investigation of trailing edge noise reduction using novel serrations," *19th AIAA/CEAS Aeroacoustics Conference*, AIAA-2013-2009.

[22]Finez, A., Jondeau, E., Roger, M., and Jacob, M., "Broadband noise reduction with trailing edge brushes," *16th AIAA/CEAS Aeroacoustics Conference, Stockholm, Sweden*, AIAA-2010-3980.

[23]Herr, M. and Dobrzynski, W., "Experimental Investigations in Low-Noise Trailing-Edge Design," *AIAA Journal*, Vol. 43(6), 2005, pp. 1167–1175.

[24]Ali, S. A. S., Azarpeyvand, M., and da Silva, C. R. I., "Trailing-edge flow and noise control using porous treatments," *Journal of Fluid Mechanics*, Vol. 850, 2018, pp. 83–119.

[25]Showkat Ali, S. A., Azarpeyvand, M., Szőke, M., and Ilário da Silva, C. R., "Boundary layer flow interaction with a permeable wall," *Physics of Fluids*, Vol. 30, No. 8, 2018, pp. 085111.

[26]Showkat Ali, S. A., Szőke, M., Azarpeyvand, M., and Ilario da Silva, C. R., "Turbulent Flow Interaction with Porous Surfaces," *2018 AIAA/CEAS Aeroacoustics Conference*, 2018, p. 2801.

[27]Showkat Ali, S. A., Azarpeyvand, M., and Ilario da Silva, C. R., "Experimental study of porous treatment for aerodynamic and aeroacoustic purposes," *23rd AIAA/CEAS Aeroacoustics Conference*, 2017, p. 3358.

[28]Geyer, T., Sarradj, E., and Fritzsche, C., "Porous airfoils: noise reduction and boundary layer effects," *15th AIAA/CEAS Aeroacoustics Conference*, No. May, 2009, pp. 1–18.

[29]Geyer, T., Sarradj, E., and Fritzsche, C., "Measurement of the noise generation at the trailing edge of porous airfoils," *Experiments in Fluids*, Vol. 48, No. 2, 2010, pp. 291–308.

[30]Showkat Ali, S., Liu, X., and Azarpeyvand, M., "Bluff Body Flow and Noise Control Using Porous Media," *22nd AIAA/CEAS Aeroacoustics Conference, Lyon, France*, AIAA-2016-2754.

[31]Showkat Ali, S. A., Szőke, M., and Azarpeyvand, M., "Trailing Edge Bluntness Flow and Noise Control Using Porous Treatments," *22nd AIAA/CEAS Aeroacoustics Conference, Lyon, France*, AIAA-2016-2832.

[32]Liu, H., Azarpeyvand, M., Weia, J., and Qua, Z., "Tandem cylinder aerodynamic sound control using porous coating," *Journal of Sound and Vibration*, , No. 334, 2014, pp. 190–201.

[33]Afshari, A., Azarpeyvand, M., Dehghan, A. A., and Szőke, M., "Trailing Edge Noise Reduction Using Novel Surface Treatments," *22nd AIAA/CEAS Aeroacoustics Conference, Lyon, France*, AIAA-2016-2834.

[34]Afshari, A., Azarpeyvand, M., Dehghan, A. A., and Szőke, M., "Three-Dimensional Surface Treatments for Trailing Edge Noise Reduction," *23rd International Congress on Sound & Vibration, Athens, Greece*, 2016.

[35]Clark, I., Baker, D., Alexander, W. N., Devenport, W., Glegg, S. A., Jaworski, J., and Peake, N., "Experimental and Theoretical Analysis of Bio-Inspired Trailing Edge Noise Control Devices," *22nd AIAA/CEAS Aeroacoustics Conference*, 2016, p. 3020.

[36]Clark, I., Alexander, W. N., Devenport, W., Glegg, S. A., Jaworski, J., Daily, C., and Peake, N., "Bio-Inspired Trailing Edge Noise Control," *21nd AIAA/CEAS Aeroacoustics Conference*, 2015, p. 2365.

[37]Ai, Q., Azarpeyvand, M., Lachenal, X., and Weaver, P. M., "Aerodynamic and aeroacoustic performance of airfoils with morphing structures," *Wind Energy*, Vol. 19, No. 7, 2016, pp. 1325–1339.

[38]Antonia, R. A., Fulachier, L., Krishnamorthy, L. V., Benabid, T., and Anselmet, F., "Influence of wall suction on the organized motion in a turbulent boundary layer," *Journal of Fluid Mechanics*, Vol. 190, 1988, pp. 217–240.

[39]Antonia, R. A., Zhu, Y., and Sokolov, M., "Effect of concentrated wall suction on a turbulent boundary layer," *Physics of Fluids*, Vol. 7, No. 10, 1995, pp. 2465–2474.

[40]Oyewola, O., Djenidi, L., and Antonia, R., "Influence of localised double suction on a turbulent boundary layer," *Journal of Fluids and Structures*, Vol. 23, No. 5, 2007, pp. 787 – 798.

[41]Oyewola, O., Djenidi, L., and Antonia, R. A., "Influence of localised wall suction on the anisotropy of the Reynolds stress tensor in a turbulent boundary layer," *Experiments in Fluids*, Vol. 37, No. 2, 2004, pp. 187–193.

[42]Oyewola, O., Djenidi, L., and Antonia, R., "Combined influence of the Reynolds number and localised wall suction on a turbulent boundary layer," *Experiments in Fluids*, Vol. 35, No. 2, 2003, pp. 199–206.

[43]Djenidi, L., Agrawal, A., and Antonia, R., "Anisotropy measurements in the boundary layer over a flat plate with suction," *Experimental Thermal and Fluid Science*, Vol. 33, No. 7, 2009, pp. 1106 – 1111.

[44]Park, J. and Choi, H., "Effects of uniform blowing or suction from a spanwise slot on a turbulent boundary layer flow," *Physics of Fluids*, Vol. 11, 1999, pp. 3095.

[45]Wolf, A., Lutz, T., Würz, W., Krämer, E., Stalnov, O., and Seifert, A., "Trailing edge noise reduction of wind turbine blades by active flow control," *Wind Energy*, Vol. 1737, 2014.

[46]Lutz, T., Arnold, B., Wolf, A., and Krämer, E., "Numerical Studies on a Rotor with Distributed Suction for Noise Reduction," *Journal of Physics: Conference Series*, Vol. 524, No. 1, 2014, pp. 012122.

[47]Matera, D., *Validation of the noise prediction code Rnoise and reduction of trailing edge noise by active flow control*, Ph.D. thesis, Universita Degli Studi Di Padova, 2013.

[48]Arnold, B., Rautmann, C., Lutz, T., and Kraemer, E., "Design of a Boundary-Layer Suction System for Trailing-Edge Noise Reduction of an Industrial Wind Turbine," *35th Wind Energy Symposium*, AIAA-2017-1380.

[49]Arnold, B., Lutz, T., Krämer, E., and Rautmann, C., "Wind-Turbine Trailing-Edge Noise Reduction by Means of Boundary-Layer Suction," *AIAA Journal*, Vol. 56(5), 2018, pp. 1843–1854.

[50]Plogmann, B. and Würz, W., "Aeroacoustic measurements on a NACA 0012 applying the Coherent Particle Velocity method," *Experiments in Fluids*, Vol. 54, No. 7, 2013, pp. 1556.

[51]Kline, S. J. and McClintock, F. A., "Describing uncertainties in single-sample experiments," *Mechanical Engineering*, Vol. 75, No. 1, Jan 1953, pp. 3–8.

[52]Schewe, G., "On the structure and resolution of wall-pressure fluctuations associated with turbulent boundary-layer flow," *Journal of Fluid Mechanics*, Vol. 134, 9 1983, pp. 311–328.

[53]Gray, R. M. and Goodman, J. W., *Fourier transforms: an introduction for engineers*, Vol. 322, Springer Science & Business Media, 2012.

[54]Spalding, D., "A single formula for the law of the wall," *Journal of Applied Mechanics*, Vol. 28, No. 3, 1961, pp. 455–458.

[55]Schlatter, P. and Örlü, R., "Assessment of direct numerical simulation data of turbulent boundary layers," *Journal of Fluid Mechanics*, Vol. 659, 2010, pp. 116–126.